LASER DOPPLER FLOWMETERS PROTOTYPES VALIDATION USING MONTE CARLO SIMULATIONS

Edite Figueiras[1], Rita Campos[1], Ricardo Oliveira[1], Luís F. Requicha Ferreira[1], Frits de Mul[2]
and Anne Humeau-Heurtier[3]

[1]*Instrumentation Center (GEI-CI), Physics Department, Faculty of Sciences and Technology of Coimbra University*
Rua Larga, 3004-516, Coimbra, Portugal
[2]*University of Twente, Department of Applied Physics, Biomedical Optics Group, Enschede, Netherlands*
[3]*Laboratoire d'Ingénierie des Systèmes Automatisés (LISA), Université d'Angers*
62 avenue Notre Dame du Lac, 49000 Angers, France

Keywords: Laser doppler flowmetry, Monte carlo simulations, Microcirculation.

Abstract: Two new laser Doppler flowmeter prototypes are herein validated with Monte Carlo simulations. The first prototype is a multi-wavelength laser Doppler flowmeter with different spaced detection fibres that will add depth discrimination capabilities to LDF skin monitoring. The other prototype is a self-mixing based laser Doppler flowmeter for brain perfusion estimation. In order to validate these two prototypes, Monte Carlo simulations are performed. For the first prototype validation, Monte Carlo simulations in a phantom consisting of moving fluid (pumped milk) at six different depths as well as in a skin model are proposed. For this prototype, the results show that the first order moment of the photocurrent power spectrum (M1) and mean depth measured both increase with the fibre distances tested. Moreover, M1 increases with the concentration of milk, whereas the mean depth measured decreases with the milk concentration for the phantom results. Furthermore, we show that increasing the wavelength of incoming light, in the skin model, increases the mean depth probed. For the second prototype validation, Monte Carlo simulations are carried out on a rat brain model. We show that the mean measurement depth in the rat brain with our probe is 0.15 mm.

1 INTRODUCTION

Laser Doppler flowmetry (LDF) is a Doppler Effect-based technique used for microcirculation blood flow monitoring where monochromatic light, guided by optical fibres, is transmitted to the tissues under study. In the tissues the laser light can be reflected, absorbed, transmitted or scattered. The photons scattered by moving particles, like red blood cells (RBCs), are frequency shifted in accordance with the Doppler Effect. These photons get red blood cells velocity information. If they are detected, together with static particles scattered photons, they will produce a stochastic photocurrent in the photodetector. This photocurrent is related with the velocity and concentration of the RBCs (Bonner and Nossal, 1981); (Humeau et al., 2007).

Currently, LDF does not give any absolute measure of blood perfusion, i.e. it is not possible to express the flux signal in absolute flow units,

because variables as the sampled volume, the photons path-length, the direction of the blood flow, and the amount of blood vessels and their length in the measuring volume are unknown (Nilsson et al., 2003); (Morales, 2005). For that reason, LDF signals collected in different tissues cannot be directly compared. Moreover, LDF signals recorded from human skin lack in estimating the sampling depth. These difficulties lead to ambiguities in the discrimination of the fraction of light scattered from superficial and deeper blood microcirculation skin layers (Oliveira et al., 2011). Besides this, commercial available flowmeters use different signal processing algorithms and calibration procedures making impossible the comparison of their results (Nilsson et al., 2003); (Morales, 2005). Concerning LDF invasive measurements, the smallest commercial probes available (with 450 μm diameter) are too large for research studies in small organs of animals as rat brain, causing damage in an

extension that may negatively impact local measurements (Oliveira et al., 2011).

Monte Carlo methods are statistic methods used in stochastic simulations with applications in several areas as physics, mathematics, and biology. Monte Carlo simulations of light transport are very helpful in photon propagation studies in turbid media, as skin. They have been widely used in LDF area (see for example Figueiras et al., 2011). In Monte Carlo methods, the light transport in turbid media is based on the simulation of the photon trajectories, where separate photons travel through the tissues. Several phenomena as scattering, absorption and refraction can be simulated based on the scattering functions, Fresnel relations, etc.

We present herein Monte Carlo simulations results for validation of two new laser Doppler flowmeter prototypes. These prototypes have been built in order to eliminate two drawbacks existing in the LDF technique. The first prototype aims at giving depth perfusion measurements information (non invasive prototype) for human skin. The second prototype aims at reducing the size of LDF invasive probes for rat brain measurements (invasive prototype). For the first prototype validation, Monte Carlo simulations in a phantom consisting of moving fluid at six different depths are herein proposed. Simulations in a skin model are also presented. For the second prototype validation, Monte Carlo simulations are carried out on a rat brain model. In what follows, we first present the two prototypes and the three simulated models. Finally, the Monte Carlo simulations are detailed and the computed signals are presented.

2 MATERIALS AND METHODS

2.1 Prototypes

Skin microcirculation is present in the dermis and is organized into two horizontal plexuses: the most superficial is situated in the papillary dermis at 0.4 - 0.5 mm below the skin surface; the second plexus is located at the dermal subcutaneous interface at 1.9 mm from the skin surface where arteriovenous anastomoses can be found (Brevarman, 2000); (Roustit et al., 2008). A new laser Doppler flowmeter prototype with depth discrimination capabilities is being built in order to determine the sampling depth of the backscattered photons used to compute the LDF signal (Oliveira et al., 2011). This prototype is a non-invasive and multi-wavelength prototype device, with 635, 785, and 830 nm laser

wavelengths. The probe used is from Perimed® AB and has a central emitting fibre and collecting fibres located at 0.14, 0.25 and 1.2 mm from the emitting fibre (Oliveira et al., 2011).

A self-mixing based prototype with a miniaturized laser Doppler probe is also being built in order to monitor blood flow changes in rat deep brain structures without causing significant damage to the tissue (Oliveira et al., 2011). In self-mixing method, the monitor photodiode at the rear face of the laser diode is used for signal detection; a single optical fibre is therefore used for light emission and detection. Pigtailed laser diodes, with 785 and 1308 nm laser wavelengths and with single mode optical fibre are used. Standard single mode optical fibres have 125 and 250 μm of cladding and jacket diameters, respectively. The probe consists of the stripped optical fibre inserted in a micro-needle with an outer diameter of 260 μm (Oliveira et al., 2011). Measurements will be made in the rat brain hippocampus. As commercial available probes have a 450 μm diameter, the use of only one optical fibre allows us to reduce the size of the probe to 58%.

2.2 Phantom and Simulation Models

2.2.1 Phantom Model

The phantom model was built with the purpose to evaluate, *in vitro*, the non-invasive flowmeter prototype response to moving fluid at different depths (as it can be found in skin) (Figueiras et al., 2010). The phantom consists of a Teflon® microtube rolled around an aluminium metal piece with a total of six layers. The inner and outer diameters of the microtube are 0.3 and 0.76 mm, respectively. Commercial skimmed milk has been chosen as a moving fluid because it has various components that act as scatterers, namely carbohydrates, fat, and protein. Moreover, it does not sediment like microspheres, and it has similar behaviour to intralipid solutions (Waterworth et al., 1995). Finally, milk is easier for handling than blood and, besides, it is cheaper. However, as milk is unstable, we use the same milk solution for one day only. Milk is pumped in the microtubes with a motorized syringe with different velocities: 1.56, 3.12, 4.68, 6.25, 7.78, and 9.35 mm/s. Different milk solutions were used: 100% milk, and aqueous solutions with 50% and 25% of milk.

The first simulated model (presented in figure 1) consists of three main layers. The first layer is composed of a set of objects equivalent to the six microtube layers and it has a total depth of 5 mm.

The two deeper layers mimic the aluminium plate and have a thickness of 0.1 mm each one: one acts as a scatterer with isotropic semi-spherical backscattering and the other is a totally reflecting layer. The laser light was considered as a pencil beam shape and it was positioned at the top of the most superficial tube. A parabolic profile was used for the milk flow simulations where the maximum velocity is twice the mean velocity.
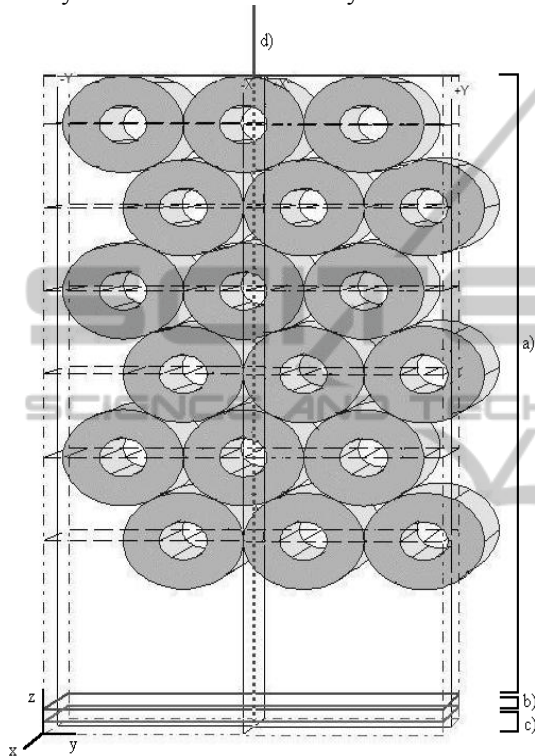

Figure 1: Simulation phantom model: it consists of three main layers: a) the upper layer, composed of microtubes with skimmed milk as moving fluid; and the two deeper layers, b) and c) mimic the aluminium plate. d) represents the laser beam.

The simulations were made only for 635 nm laser light wavelength due to the absence of information concerning milk and Teflon optical properties for 785 and 830 nm laser light. The milk optical properties used were published by Waterworth et al. (1995), where the refractive index for milk is 1.346, absorption (μ_a) and scattering coefficients (μ_s) are 0.00052 and 52 mm^{-1}, respectively. The Teflon optical properties used were published by Li et al. (2008) where the refractive index is 1.367, $\mu_a = 0.001$ mm^{-1} and $\mu_s = 167$ mm^{-1}, respectively. Henyey-Greenstein phase function was used with $g = 0.90$ for both components (Waterworth et al., 1995; Li et al., 2008).

Simulations were made for six different velocities for milk speed, three different milk solutions and three different detection distances, which gives a total of 54 simulations, with 5,000,000 photons detected in each simulation.

2.2.2 Skin Model

The skin simulations were made for three wavelengths (635, 785 and 830 nm) and three different emitting-receiving fibre separations (0.14. 0.25 and 1.2 mm), the ones used in the non self-mixing prototype.

The skin model was based in the model presented by Fredriksson et al. (2008; 2009). It consists of 6 layers with different thicknesses and a given blood concentration at three different flow velocities with random direction (see table 2 from Fredriksson et al., 2009). Oxygenated blood with hematocrit equal to 42% was considered (normal hematocrit values: 36-44% for females; 39-50% for males). A parabolic distribution was considered for the blood velocities.

The skin and blood optical properties for 635 and 785 nm were also based on Fredriksson et al. (2009), whereas for 830 nm they were based on the results presented by Simpson et al. (1998) and Prahl (1999).

The skin and blood optical properties are summarized in table 1. Concerning the scattering functions, the blood was modelled with the Gegenbauer kernel scattering phase function, with $\alpha_{GK} = 1$ for all wavelengths and $g_{GK} = 0.95$ mm^{-1} for 635 nm and $g_{GK} = 0.948$ mm^{-1} for 785 and 830 nm. For static tissue the Henyey-Greenstein phase function was used with $g = 0.85$ mm^{-1}. The refractive index was set to 1.4 for all skin layers, 1.58 for the probe and 1 for the surrounding air.

The laser light was simulated as an external photon beam, with pencil beam shape with a perpendicular entrance in the tissue and the path tracking was recorded with $1/\mu'_s$ resolution (μ'_s refers to the reduced scattering coefficient). The numerical aperture (NA) of the fibres is 0.37. A total of 3 times 4 simulations were made where 10,000,000 photons were detected in each one.

The optical properties of deoxygenated and oxygenated blood are equal except for the absorption coefficient (see table 5 of Fredriksson et al., 2009).

However, this value is rather independent of the level of oxygenation of the blood, once the chosen wavelengths are close to the 800 nm isobestic point of oxygenated and deoxygenated haemoglobin.

Table 1: Optical properties for the six skin layers and oxygenated blood (hematocrit=42%) used in skin simulations for 635, 785 and 830 nm.

Wavelength (nm)	μ_a (mm^{-1})			μ'_s (mm^{-1})			g		
	635	785	830	635	785	830	635	785	830
Epidermis	0.15	0.1	0.0122	4.8	3.5	1.81	0.85	0.85	0.9
Papillary dermis	0.15	0.1	0.0122	3	2	1.81	0.85	0.85	0.9
Superior blood net	0.15	0.1	0.0122	3	2	1.81	0.85	0.85	0.9
Reticular dermis	0.15	0.1	0.0122	3	2	1.81	0.85	0.85	0.9
Inferior blood net	0.15	0.1	0.0122	3	2	1.81	0.85	0.85	0.9
Subcutis	0.15	0.1	0.00856	2.4	2	1.12	0.85	0.85	0.9
Blood	0.34	0.5	0.52	2.13	2	2	0.991	0.991	0.991

2.2.3 Rat Brain Model

The rat hippocampus consists of several substances such as grey matter, white matter and blood vessels, among others. The blood percentage is nearly 4.5% and the white matter is up to 4% of the blood volume. As the percentage of white matter is very low we considered that the hippocampus has 95.5% of grey matter and 4.5% of blood (3.6% of oxygenated blood and 0.9% of deoxygenated blood) (Fredriksson et al., 2009); (Hamberg et al., 1996).

The optical properties chosen in the simulations for the 785 nm wavelength were based on Fredriksson et al. (2009). The absorption coefficients used were 0.2, 0.5 and 0.64 mm^{-1} for grey matter, oxygenated and deoxygenated blood, respectively. The scattering coefficients were 0.78 mm^{-1} for the grey matter and 2 mm^{-1} for oxygenated and deoxygenated blood and the anisotropy factor was 0.900 for grey matter and 0.991 for oxygenated and deoxygenated blood (Fredriksson et al., 2009). Concerning the scattering functions, the blood (oxygenated and deoxygenated) was modeled with the Gegenbauer kernel scattering phase function, with $\alpha = 1$ and g = 0.948 mm-1 (Fredriksson et al., 2009). For grey matter the Henyey-Greenstein phase function was used with g = 0.85 mm^{-1} (Fredriksson et al., 2009). For blood a hematocrit equal to 42% was considered. The refractive index was set to 1.4 to all components and the laser light was simulated as a pencil beam with a perpendicular entrance in the tissue. The path tracking was recorded with $1/\mu'_s$ resolution, where μ'_s is the reduced scattering coefficient. The numerical aperture (NA) of the optical fibres is 0.11.

The simulations were performed only for the 785 nm laser light wavelength due to the absence of information concerning optical properties of grey matter, oxygenated and deoxygenated blood for the 1300 nm laser light beam.

2.2.4 Monte Carlo Simulations

For the simulations, Monte Carlo software 'MONTECARL' from Frits de Mul was used (De Mul et al., 1995); (De Mul, 2004).

3 RESULTS AND DISCUSSION

3.1 Phantom Simulations

The results obtained in the phantom model, namely the mean depth of the Doppler events per photon, the percentage of Doppler shifted photons detected and the mean of Doppler scattering events per photon are given in table 2 for 1.56 mm/s milk velocity.

The emitting-receiving fibre separation influences the measurements, in such a way that for larger fibre separations, a larger sample volume is probed. Therefore, increasing the fibre distance, photons travel through deeper objects leading to an increase in the mean depth of Doppler shifted photons. Previous studies (Fredriksson et al., 2008; Fredriksson et al., 2009) based on light propagation in tissue using Monte Carlo computational simulations are in agreement with these results. The milk concentration also influences the mean depth, which decreases with the increase of milk concentration. This is due to a higher degree of multiple Doppler shifts registered for higher milk concentrations.

The percentage of Doppler shifted photons detected increases with the emitting-receiving separation for each velocity. This is expected because when the fibre distance increases, the measured sample volume increases, and the photons

will encounter a larger amount of moving scatterers. When the concentration of milk increases the percentage of Doppler shifts detected also increases. The higher the milk concentration, higher scatterers are present, consequently, more scattering events occur.

Likewise, the mean Doppler scattering events per photon also increase with the fibre distance for each velocity. This is not surprising as we are considering a homogenous model (for the scatterers velocity and concentration). Therefore, an increase in the sampled volume will naturally lead to more Doppler scatters events. Increasing the milk concentration, a higher degree of multiple Doppler scattering is reached, because the higher the concentration, the higher the scatterers.

Similar results were obtained for all velocities in what concerns the mean depth of the Doppler events per photon, the percentage of Doppler shifted photons detected and the mean of Doppler scattering events per photon, as this parameters are independent of the velocity of the moving fluid.

The first order moment of the Doppler power spectrum, M1, was also evaluated. Figure 2 shows the effect on M1 when the fiber distance increases, for each velocity and for a milk concentration of 25%. It can be seen that higher values of M1 come from larger fiber separations whereas the lower values of M1 are obtained for 0 mm fiber separation. Another observation is that, in general, M1 increases with the velocity and with the milk concentration. This is not surprising since M1 is proportional to perfusion (Perf), which in turn is proportional to the scatterers concentration times their average velocity.

However, in some specific cases M1 does not increase with the velocity, especially for the two highest velocities for 1.2 mm fiber distance. This might be due to the phantom model that saturates in such extreme situations.

In order to better understand the path travelled by the photons, a path tracking study was done. The path tracking can be 'followed' in MC software during the simulations. In figure 3 it can be seen the path tracking for 25 [figure 3a)] and 13128 [figure 3b)] photons injected. In figure 3 b) it can be clearly seen the three layers (cf. figure 1). The average number of paths travelled by each photon and the respective average depth were estimated. Furthermore, the average path length for each photon was also evaluated.
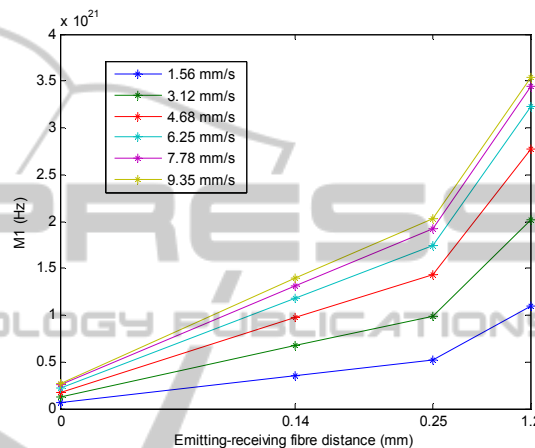

Figure 2: M1 *vs.* emitting-receiving fibre distance, on the phantom model with 25% milk concentration for 635 nm laser light wavelength.

The results for 1.56 mm/s are presented in table 3. The results are similar for all simulated velocities because these parameters are independent of the scatterers velocity. For different milk concentrations, there is not a clear tendency for the variation of the number of paths with the milk concentration.

The average number of paths for each photon increases with emitting-receiving fibre distance (cf. table 3).

Table 2: The mean depth of the Doppler events for each photon, the percentage of Doppler shifted photons detected and the mean of Doppler scattering events per photon for the phantom model, with milk pumped at 1.56 mm/s, for 635 nm laser light wavelength.

Fibre distance (mm)	Mean Doppler depth (mm)			Detected Doppler (%)			Mean Doppler scattering		
	Milk concentration			Milk concentration			Milk concentration		
	25 %	50%	100%	25%	50%	100%	25 %	50%	100%
0	0.36	0.34	0.32	4.77	6.73	10.27	3.48	5.85	10.08
0.14	0.41	0.39	0.35	26	32.35	41.26	4.29	7.30	12.66
0.25	0.43	0.40	0.37	41.23	47.76	56.45	4.37	7.78	14.27
1.2	0.56	0.55	0.53	82	86	87.47	6.47	12.65	26-63

This is expected because as mentioned, a greater fibre distance allows sampling a greater volume and therefore, a bigger number of paths are registered.

The average path depth and the average path length for each photon are the highest for 0 mm emitting-receiving fibre distances, and they are the lowest for 0.14 and 0.25 mm fibre distance. The origin of this non-linearity is unclear for the moment.

3.2 Skin Simulations

The mean depth of the Doppler events per photon, the percentage of Doppler shifted photons detected

and the mean of Doppler scattering events per photon obtained in Monte Carlo simulations, for the skin model, are presented in table 4.

The mean depth for the Doppler events, the percentage of Doppler shifted photons detected and the mean Doppler scattering per photon increase with fibre distance, as for the phantom model, because a larger emitting-receiving separation allows sampling a larger volume.

Furthermore, the mean measurement depth also increases with the wavelength. This is due to both skin absorption and scattering coefficients decrease with the wavelength, allowing the photons to travel a longer path. Similar results were obtained by
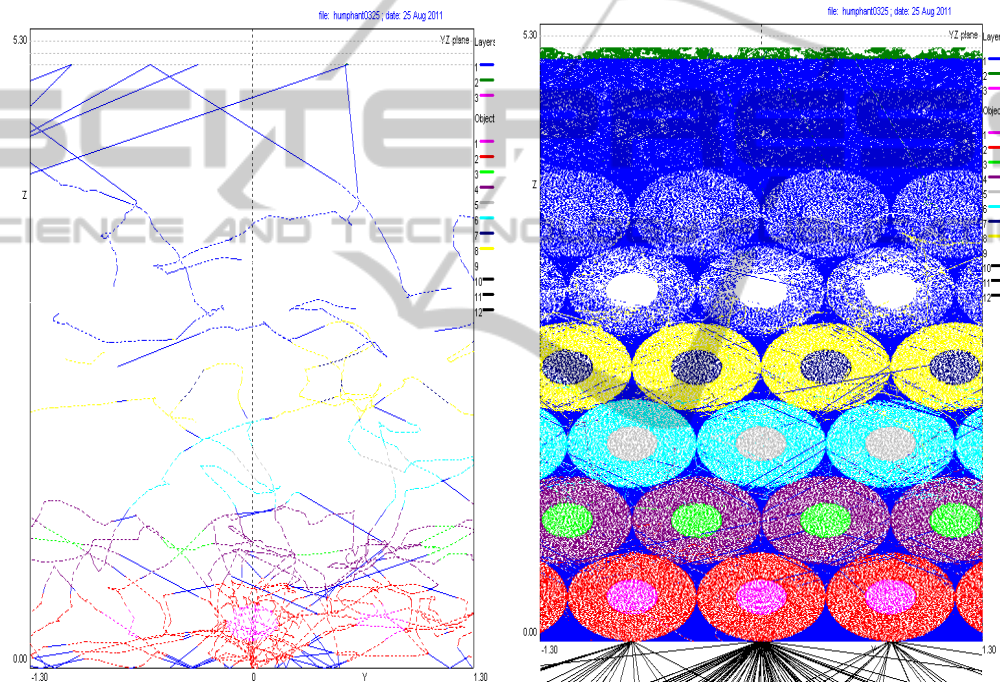

Figure 3: Path tracking registered during the simulations for: a) 25 and b) 13128 photons injected.

Table 3: Average mean path number, mean path depth and mean path length for photons for the phantom model, with milk pumped at 1.56 mm/s.

Milk concentration	Fibre distance (mm)	\<Path number\>	\<Path depth\> (mm)	\<Path length\> (mm)
5%	0	3.31	1.45	10.66
	0.14	7.00	0.23	2.53
	0.25	9.66	0.23	2.55
	1.2	25.67	0.47	5.95
50%	0	3.37	1.41	10.74
	0.14	7.06	0.24	2.58
	0.25	9.51	0.22	2.45
	1.2	25.91	0.47	6.07
100%	0	3.49	1.41	10.43
	0.14	7.04	0.22	2.53
	0.25	9.53	0.21	2.43
	1.2	27.67	0.45	6.24

Fredriksson et al. (2009), with a measurement depth slightly smaller, but with the same order of magnitude. It can be noticed that the mean depth of the Doppler shifted photons never reaches the reticular dermis or the layers below this one, since reticular dermis lies at a depth of 1.175 mm and the mean depth predicted for the Doppler events is always lower than this value. In addition, detected photons reached the superior blood net dermis only when detected with the 1.2 mm fibre distance.

The percentage of Doppler shifted detected photons also increases with the wavelength excluding for the 1.2 mm emitting-receiving fibre distance. This may be related to the distribution of the Doppler events percentage in each layer (cf. table 5). It can be seen that the reticular dermis is the 2nd layer with the most detected Doppler photons for 1.2 mm fibre distance (for 785 and 830 nm laser light), whereas for the other fibre distances the 2nd layer with the most detected Doppler photons is the papillary dermis.

This proves that the photons detected at 1.2 mm from the emitting fibre cross a higher volume of blood. Besides, the Doppler events percentage in the inferior blood net (for 1.2 mm fibre distance) decreases going from 635 to 785 nm laser light and increases going from 785 to 830 nm laser light. This layer has the second higher blood concentration when compared with the other layers. Together, with the higher volume of blood crossed and the increasing of the blood absorption coefficient with the wavelength may cause this nonlinearity.

In opposition, the mean Doppler scattering event does not follow a general trend when increasing the wavelength of the incident light but is always smaller than 1.5, which means that there are few photons that suffer multiple Doppler shifts.

Simulation results also demonstrate that M1 increases with the emitting-receiving fibre distance (see table 6). Since M1 is proportional to the concentration of moving RBCs times its average velocity, and both parameters increase with the fibre distance, this was expected.

Table 4: The mean depth of the Doppler events for each photon, the percentage of Doppler events detected and the mean of Doppler scattering events per photon for the skin model.

Fibre distance (mm)	Mean depth Doppler (mm)			Detected Doppler (%)			Mean Doppler scattering		
	Wavelength (nm)			Wavelength (nm)			Wavelength (nm)		
	635	785	830	635	785	830	635	785	830
0	0.24	0.25	0.27	1.94	1.97	3.54	1.19	1.16	1.15
0.14	0.27	0.29	0.31	9.62	10.71	14.54	1.23	1.22	1.23
0.25	0.28	0.30	0.33	15.45	16.29	20.39	1.26	1.23	1.25
1.2	0.37	0.38	0.41	47.7	41.89	43.45	1.49	1.41	1.46

Table 5: Doppler events percentage in each layer for the skin model.

Wavelength (nm)	Fibre Distance (mm)	Skin layers					
		Epidermis	Papillary dermis	Superior blood net	Reticular dermis	Inferior blood net	Subcutis
635	0	0	41.07	51.19	7.24	0.5	0
	0.14	0	35.1	53.06	10.31	1.37	0.17
	0.25	0	31.98	55.23	11.1	1.49	0.21
	1.2	0	19.43	56.21	19.51	4.08	0.77
785	0	0	41.73	48.84	8.93	0.51	0
	0.14	0	30.85	54.86	12.97	1.33	0
	0.25	0	27.69	56.42	14.38	1.51	0
	1.2	0	18.81	55.44	22.24	3.51	0
830	0	0	38.76	49.36	10.35	1.54	0
	0.14	0	26.66	55.91	15.09	2.33	0
	0.25	0	23.09	57.05	17.27	2.59	0
	1.2	0	16.57	53.06	25.15	5.21	0

In what concerns the wavelengths, M1 firstly decreases from 635 to 785 nm and then increases for 830 nm. This can be explained if we look at the Doppler photons percentage that exceeds the reticular dermis. This percentage is higher for 830 nm followed by 635 nm and lower for 785 nm, with the exception of the 0 mm fibre distance (Table 5). As the inferior blood net has the highest concentration of the high velocity component of RBCs (30 mm/s), it results in a higher Doppler shifts for 635 nm than for 785 nm photons. Therefore M1 will be higher for 635 nm than for 785 nm.

Table 7 shows the results of the path tracking study for the skin model. It can be observed that the average path number travelled by each photon, the mean path depth and the average path length increase with emitting-receiving fibre distance. This occurs, because increasing the fibre distance a greater tissue volume is probed, and so, more scattering events occur. The mean path number does not follow a general trend when increasing the wavelength of the incident light.

The path depth increases with the laser light wavelength due to both skin absorption and scattering coefficients decrease with the wavelength, allowing the photons to travel a longer path. This is in agreement with the mean depth of Doppler events results showed in table 4. The average path length increases with the wavelength, excluding for the 1.2 mm emitting-receiving fibre distance. This may be related with the distribution of the Doppler events percentage in each layer (cf. table 5) as discussed later when the percentage of Doppler shifted detected photons is analyzed.

3.3 Rat Brain Simulations

In the simulation made for rat brain model, it can be seen that the photons Doppler shifted travelled a mean depth of 0.15 mm (cf. table 8). This value is in accordance with Frediksson et al. (2009) which obtained 0.16 mm of measurement depth. Each photon suffers, in average, 2.23 scatters events. In a total of 5,000,000 photons detected 11.9% had

Table 6: First order moment of Doppler power spectrum (M1) for skin model.

Wavelength (nm)	M1 (Hz)			
	Fibre distance (mm)			
	0	0.14	0.25	1.2
635	3.57E+18	2.51E+19	3.71E+19	1.63E+20
785	3.45E+18	2.13E+19	3.23E+19	1.05E+20
830	5.30E+18	2.66E+19	3.93E+19	1.06E+20

Table 7: Mean path number, mean path depth and mean path length for photons, using the skin model.

Wavelength (nm)	Fibre distance (mm)	<Path number>	<Path depth> (mm)	<Path length> (mm)
635	0	3.16	0.02	0.23
	0.14	6.1959	0.0775	0.78
	0.25	7.99	0.11	1.16
	1.2	19.77	0.27	4.11
785	0	3.08	0.02	0.23
	0.14	5.98	0.09	0.86
	0.25	7.46	0.12	1.26
	1.2	14.71	0.26	3.65
830	0	3.77	0.04	0.34
	0.14	6.93	0.12	1.12
	0.25	8.34	0.16	1.57
	1.2	14.86	0.28	4.01

Table 8: The percentage of Doppler events detected the mean of Doppler scattering, the mean depth of the Doppler events for each photon and M1 for the rat model.

Mean depth Doppler (mm)	Detected Doppler (%)	Mean Doppler scattering	M1 (Hz)
0.15	11.9	2.23	3.51E+17

suffered Doppler shift and M1 was predicted to be 3.51E+17 Hz. These results will help in the rat brain probe positioning as it shall be 0.15 mm above the mean measurement depth.

4 CONCLUSIONS

Monte Carlo simulations used for the two new LDF prototypes validation showed results in accordance with the literature. For the non invasive prototype, the phantom model presented here to evaluate the *in vitro* prototype response, has shown good agreement with theoretical expectations. M1 increases with the concentration and with the fibre distances. The mean depth increases with the fibre distance and decreases with the milk concentration. For *in vivo* evaluation, the estimated parameters for the skin model corresponded to *a priori* expectations. We have shown that increasing the wavelength of incoming light (in the range of 635-830 nm) increases the mean depth probed. Moreover, an increase of the source-detection fibre separations leads to a higher mean depth and M1 value. In what concerns the rat brain model, the mean depth that photons Doppler shifted travel was estimated to be 0.15 mm which is in agreement with the literature.

ACKNOWLEDGEMENTS

REFERENCES

Bonner, R. F., Nossal, R. (1981). Model for laser Doppler measurements of blood flow in tissue. *Applied Optics*; 20,2097–2107.

Braverman, I. M.(2000). The Cutaneous Microcirculation. *J Investig Dermatol Symp Proc*; 5, 3-9.

De Mul, F. F. M., Koelink, M. H., Kok, M. L., Harmsma, P. J., Greve, J., Graaff, R. and Aarnoudse, J. G. (1995). Laser Doppler Velocimetry and Monte Carlo Simulations on Models for Blood Perfusion in Tissue. *Applied Optics*; 34, 6595-6611.

De Mul, F. F. M, 2004. Monte-Carlo simulation of Light transport in Turbid Media. In *Handbook of Coherent Domain Optical Methods, Biomedical Diagnostics, Environment and Material Science* (chapter 12), Tuchin, V. V. (Ed.). Dordrecht: Kluwer Publishers.

Figueiras, E., Loureiro, V., Ferreira, L. F. R. and Humeau, A. (2009). Some Reasons to Build a New Laser Doppler Flowmeter to Monitor Microvascular Blood Flow. *IFMBE Proceedings, World Congress on Medical Physics and Biomedical Engineering*; 25/IV, 1865-1868, Munich (Germany).

Figueiras, E., Ferreira, L. F. R. and Humeau, A. (2010). Phantom validation for depth assessment in laser Doppler flowmetry technique. *Proceedings of EOS, Topical Meeting on Diffractive Optics*; 2413, Koli (Finland).

Figueiras, E., Ferreira, L. F. R., De Mul, F. F. M. And Humeau, A. (2011). *Monte Carlo Methods to Numerically Simulate Signals Reflecting the Microvascular Perfusion*. In *Numerical Simulations - Applications, Examples and Theory* (Chapter 7), Angermann, L. (Ed.). Rijeka: InTech. Available from: http://www.intechopen.com/articles/show/title/monte-carlo-methods-to-numerically-simulate-signals-reflecting-the-microvascular-perfusion

Fredriksson, I., Larsson, M. and Strömberg, T. (2008). Optical microcirculatory skin model: assessed by Monte Carlo simulations paired with *in vivo* lased Doppler flowmetry. *Journal of biomedical optics*; 13,014015.

Fredriksson, I., Larsson, M. and Strömberg, T. (2009). Measurement depth and volume in laser Doppler flowmetry. *Microvascular research*; 78,4-13.

Hamberg, L. M., Hunter, G. J., Kierstead, D., Lo, E. H., Gonzalez, R. G. and Wolf, G. I. (1996). Measurement of cerebral blood volume with substraction three-dimentional functional CT. *Am. J. Neuroradiol;* 17(10), 1861-1869.

Humeau, A., Steenbergen, W., Nilsson, H. and Strömberg, T. (2007). Laser Doppler perfusion monitoring and imaging: novel approaches, *Med. Biol. Eng. Comput.*, 45, 421-435.

Li, Q., Lee, B. J., Zhang, Z. M. and Allen, D. W. (2008). Light scattering of semitransparent sintered polytetrafluoroethylene films. *Journal of Biomedical Optics*; 13(5), 054064.

Morales, F. (2005). Improving the clinical applicability of laser Doppler perfusion monitoring. PhD thesis, Universidade de Groningen.

Nilsson, G. E., Salerud, E. G., Stromberg, T. N. O. and Wardell, K. (2003). *Laser Doppler perfusion monitoring and imaging*. In Biomedical photonics

Handbook (chapter 15), Vo-Dinh, T. (Ed.). Washington, D.C.: CRC press.

Oliveira, R., Semedo, S., Figueiras, E., Requicha Ferreira, L. F., Humeau, A. (2011). Laser Doppler Flowmeters for microcirculation measurements, *1st Portuguese Meeting in Bioengineering - Bioengineering and Medical Sciences - The challenge of the XXI century, Portuguese chapter of IEEE EMBS*; Technical University of (Portugal).

Prahl, 1999. Optical Absorption of Hemoglobin. Retrived from http://omlc.ogi.edu/spectra/hemoglobin/index.html

Roustit, M., Simmons, G. H., Carpentier, P., and Cracowski, J. L. (2008). Abnormal digital neurovascular response to local heating in systemic sclerosis. *Rheumatology*; 47, 860-864.

Simpson, C. R., Kohl, M., Essenpreis, M. and Cope, M. (1998). Near infrared optical properties of ex-vivo human skin and subcutaneous tissues measured using the Monte Carlo inversion technique. *Phys Med Biol*; 43, 2465-2478.

Waterworth, M. D., Tarte, B. J., Joblin, A. J., van Doorn, T. and Niesler, H. E. (1995). Optical transmission properties of homogenized milk used as a phantom material in visible wavelength imaging. *Australasian Physical and Engineering Sciences in Medicine*;18, 39-44.